JOURNAL OF GEOPHYSICAL RESEARCH: OCEANS, VOL. 118, 3278–3291, doi:10.1002/jgrc.20231, 2013

Creation and tidal advection of a cold salinity front in Storfjorden: 1. Polynya dynamics

Ragnheid Skogseth,[1] Miles G. McPhee,[2] Frank Nilsen,[1,3] and Lars H. Smedsrud[4]

Received 13 December 2012; revised 2 May 2013; accepted 2 May 2013; published 11 July 2013.

[1] Hydrographical measurements from the Storfjorden polynya document the presence of an abrupt front in near-freezing water dividing saline water recently created by a polynya event, from less saline water originating further south. This event occurred days before the survey with estimated heat flux ~400 W m^{-2} over the polynya. Brine-enriched shelf water (BSW) is observed downslope toward deeper parts of Storfjorden, and BSW from earlier polynya events overflows the sill. Current measurements from a nearby sound, Freemansundet, document tidal currents exceeding 80 cm s^{-1} that displaced the front back and forth beneath the measurement site on fast ice ~400 m from the polynya edge. Front displacement of ~12 km is documented and mainly due to the M_2 component superimposed on a mean residual current of 0.28 m s^{-1} into the sound induced by southerly wind during the survey. Complex topography imposes baroclinic tidal currents with strong vertical shear in the fast ice-covered sound, and with significant cross-channel flow. Supercooling events indicated in the hydrographical time series, and likely enhanced frazil ice production, are associated with double-diffusive turbulent mixing when the salinity front passes. In this way, these measurements indicate a novel ice production process along the edge of tidally induced latent heat polynyas where salinity fronts are generated. Turbulence increases (decreases) during flood (ebb) due to the destabilization (stabilization) of the water column when the salinity front passes the measurement site. Double-diffusive turbulent mixing related to tidal advection of salinity front below fast ice is pursued in a companion paper.

Citation: Skogseth, R., M. G. McPhee, F. Nilsen, and L. H. Smedsrud (2013), Creation and tidal advection of a cold salinity front in Storfjorden: 1. Polynya dynamics, *J. Geophys. Res. Oceans*, *118*, 3278–3291, doi:10.1002/jgrc.20231.

1. Introduction

[2] Polynyas are areas of enhanced air-sea fluxes in winter relative to the neighboring ice-covered regions. This is caused by direct contact between the cold atmosphere and a relatively warm ocean resulting in heat exchange two orders of magnitude greater than the exchange through the ice [*Smith et al*., 1983, 1990]. Roughly half of the total exchange of heat between the Arctic Ocean and the atmosphere occurs through openings in the ice [*Maykut*, 1986]. In a future Arctic with more leads and polynyas, or thinner ice, the sea ice cannot efficiently insulate the ocean from the atmosphere. This will influence the water transformation in the Arctic Ocean and warm the Arctic atmosphere, which in turn will influence the global circulation of the ocean and atmosphere.

[3] The shallow Arctic Ocean shelves are areas of rapid water mass transformation, partly due to the presence of coastal polynyas. The two traditional categories of polynyas are latent heat polynyas, in which wind and currents drive away consolidated ice and sensible heat polynyas, in which the heat flux from warmer subsurface waters slows or eliminates the formation of ice [*Smith et al*., 1990]. In latent heat polynyas, latent heat is released as the water is transformed into ice, whereas in sensible heat polynyas oceanic heat is required to keep the surface temperature above freezing. Coastal polynyas tend to reoccur at the same geographical location each year. Common factors at these locations are shelter from drifting ice provided by coastlines, fast ice, or ice bridges [*Ingram et al*., 2002; *Williams et al*., 2007] and offshore wind and ocean currents pushing the ice away from the shelter. Strong tidal currents make an important contribution to the dynamics of many of these recurring polynyas [*Hannah et al*., 2009], either by breaking up of the land fast ice making it easier for offshore winds and currents to make a latent heat polynya [*Zyryanov et al*., 2003], or by tidal mixing driving warmer water upslope creating a

Companion to *McPhee et al.* [2013] doi:10.1002/jgrc.20261.

[1]The University Centre in Svalbard, Longyearbyen, Svalbard, Norway.
[2]McPhee Research Co, Naches, Washington, USA.
[3]Geophysical Institute, University in Bergen, Bergen, Norway.
[4]Uni Research, Bjerknes Centre for Climate Research, University in Bergen, Bergen, Norway.

Corresponding author: R. Skogseth, The University Centre in Svalbard, PO Box 156, N-9171 Longyearbyen, Norway. (Ragnheid.Skogseth@unis.no)

2169-9275/13/10.1002/jgrc.20231

sensible heat polynya [*Topham et al*., 1983]. In addition, strong tidal currents may inhibit the consolidation of frazil ice [*Daly*, 1984].

[4] The enhanced ice formation and accompanying seawater densification taking place in coastal latent heat polynyas are crucial for maintaining the Arctic halocline layer [*Aagaard et al*., 1981] and ventilating the deep oceans [*Windsor and Björk*, 2000]. Brine rejected from growing sea ice forms dense, brine-enriched shelf waters (BSWs) that accumulate near the bottom of basins and eventually spill toward the deep sea as dense plumes [*Skogseth et al*., 2008]. According to model studies [*Gawarkiewicz and Chapman*, 1995], the rapid ice growth from intense heat loss in polynyas can create localized salinity (density) fronts along the fast ice edge of the polynya due to the orders of difference in heat flux and accompanying ice formation and brine rejection in open water in the polynya and under fast ice. Strong tidal currents often present in coastal polynya locations are then likely to advect these salinity fronts under the fast ice, with significant impact on mixing beneath the fast ice, as discussed in a companion paper [*McPhee et al*., 2013]. Observations from polynyas are, in general, scarce, and apart from the Laptev Sea polynya [*Dmitrenko et al*., 2010, 2012], little data of tidal influence in polynyas can be found.

[5] Storfjorden is located between Spitsbergen, Barentsøya, and Edgeøya on the eastern side of the Svalbard Archipelago (Figure 1) and is largely isolated from heat transported toward the Arctic by the North Atlantic Current. The processes taking place here are in many ways representative of those in the Arctic shelf seas. The fjord is generally ice covered from December through June and has large shallow areas where the temperature in winter is at the freezing point over the entire water column. A recurring latent heat polynya is known to form inside Storfjorden during northeasterly winds in winter, where further heat loss leads to ice production and brine release [*Haarpaintner et al*., 2001; *Skogseth et al*., 2004], increasing the near-bottom salinity, especially in the shallow areas. The Storfjorden polynya produces typically 0.03–0.04 Sv of BSW ($T < -1.5$°C and $S > 34.8$ psu) annually [*Skogseth et al*., 2004, 2005a].

[6] In this paper, we present a hydrographical survey of the Storfjorden polynya shortly after a major polynya event, with support from atmospheric measurements and satellite imagery (section 2). Description of the various instruments used and how they were deployed are found in section 3. Results from our hydrographical survey and the profiling current meter are found in section 4, including documentation of a narrow salinity front displaced back and forth with the tide under the fast ice, and an analysis of residual tidal currents within the water column. The applicability of our findings to other Arctic polynyas and the influence of tidal current and fronts on dense water formation on shelves are discussed in section 5, before we draw our conclusions in section 6. A detailed study of tidally induced turbulence in the boundary layer under fast ice is the focus of *McPhee et al.* [2013], who present evidence for transient supercooling produced by double-diffusive turbulent mixing associated with back-and-forth advection of a sharp salinity front.

2. Large-Scale Atmospheric Forcing

[7] Meteorological data from Hopen Island were adjusted for Storfjorden (Figure 2) following *Skogseth et al*. [2004]. The data spanning from 15 to 28 March 2007

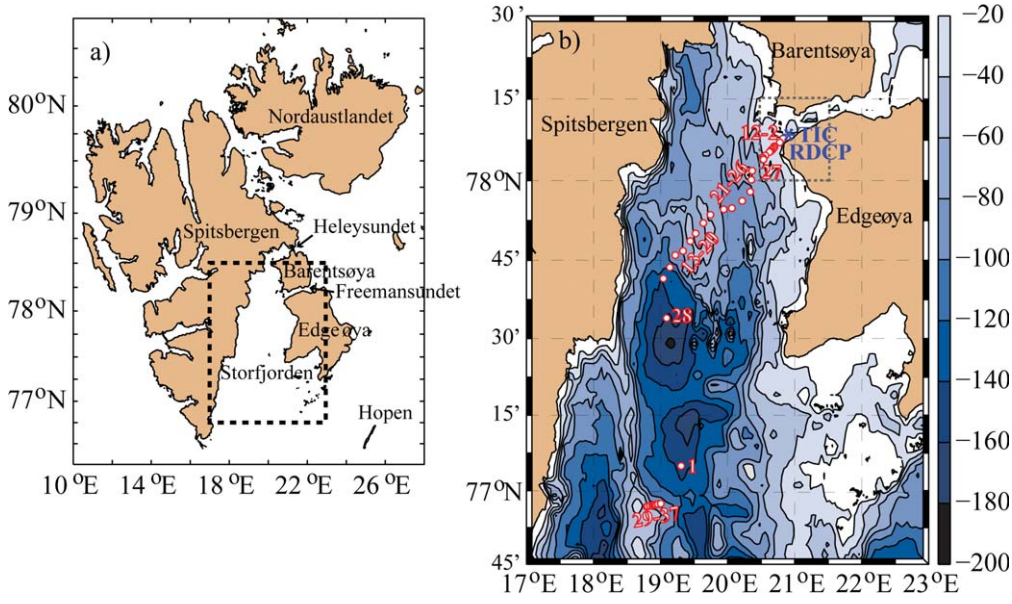

Figure 1. (a) Storfjorden in the Svalbard Archipelago with Heleysundet, FMS, and Hopen Island indicated. (b) Bathymetry map of Storfjorden as portrayed by a compiled 500 m × 500 m grid model from *Skogseth et al*. [2005b], where the ice camp (TIC and RDCP) in FMS is indicated with a blue star, and the locations of the CTD profiles are marked by white dots with red outlines and corresponding station numbers. The boxed area in Figure 1a gives the border of the map in Figure 1b, and the boxed area in Figure 1b gives the border of the map in Figure 14. Bathymetry contour is given in the colorbar.

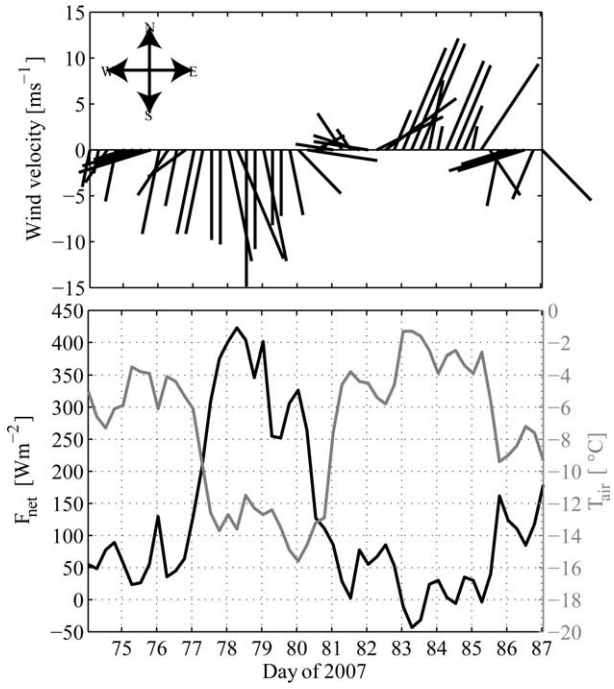

Figure 2. (upper) Stick plot of wind on Hopen Island every 6 h from 17 to 30 March 2007. (lower) Estimated net heat flux, F_{net}, from open water to atmosphere in the Storfjorden polynya and air temperature, T_{air}, from Hopen Island adjusted for Storfjorden, every 6 h from 15 to 28 March 2007.

show the meteorological conditions during the polynya event and our survey the following week. Upon our arrival in Storfjorden on 22 March (day 81), strong prevailing northerly winds up to 15 m s^{-1} pushed the pack ice out of Storfjorden creating a large polynya with accompanying frazil ice production due to low air temperatures and a large net heat flux as indicated by the estimated net heat flux exceeding 400 W m^{-2}. The net heat flux is estimated as in *Skogseth et al*. [2004] from the adjusted air temperature, wind speed and direction, cloud cover, and relative humidity from Hopen Island. Figure 3 shows a combination of Envisat ASAR (advanced synthetic aperture radar) and MODIS (Moderate Resolution Imaging Spectroradiometer) images of the Storfjorden ice cover during our cruise period. Fast ice and pack ice are easily distinguishable from the polynya and present structures of ice floes with moderate or no changes in sequential images 3 days apart. The backscatter is homogeneous (gray level). Polynyas typically include open water, frazil ice, and newly formed thin ice often involved in ridging and rafting. This gives inhomogeneous backscatter signatures inside the polynya, from very low (thin ice or calm open water) to very high (frost flowers on thin ice or wind-roughened open water). Langmuir streaks of frazil ice can be identified only under windy conditions [*Liu et al*., 1997], indicating open water. The active polynya is visible on 17 and 20 March where frazil ice streaks are clearly present in the ASAR image on 17 March. The MODIS image on 20 March shows that the polynya consists of a mixture of open water with frazil ice streaks and newly formed thin ice. When the wind turned southeasterly during 21 March (day 80) bringing warmer air masses over Storfjorden, the pack ice was pushed back into Storfjorden closing the polynya as seen in the ASAR image on 22 March. Entering Storfjorden we found thin ice cover remnants, between 5 and 20 cm, of the polynya occurring the week before. Then during 24 March (day 82), the wind turned southwesterly pushing the pack ice more eastward in Storfjorden resulting in a polynya event on the western side of Storfjorden as seen on the MODIS image on 25 March. This made it possible to make hydrographical profiles in the deeper parts of Storfjorden on our way out early on 26 March. During 26 March the wind turned northeasterly pushing the pack ice back to the western part of Storfjorden again creating a small polynya northeast in Storfjorden as seen in the ASAR image on 27 March. At the same time, the air temperature decreased accordingly.

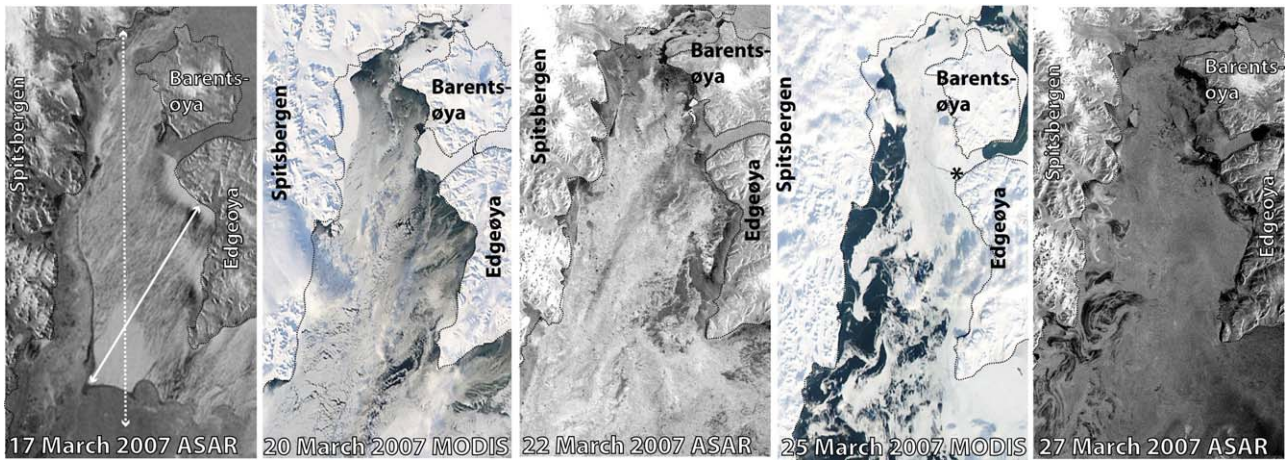

Figure 3. Envisat ASAR (synthetic aperture radar) and MODIS (optical) images of Storfjorden on 17, 20, 22, 25, and 27 March 2007 surrounded by Spitsbergen, Barentsøya, and Edgeøya with coastline indicated by the dashed black lines. The length of Storfjorden (∼190 km) is shown by the dashed white arrow, while the polynya length (∼100 km) is given by the solid white arrow on the ASAR image on 17 March. The ice camp is marked by a black star on the MODIS image on 25 March.

3. Field Measurement Campaign Description

[8] An ice camp was established on suitable fast ice at the entrance to Freemansundet (FMS) between Edgeøya and Barentsøya in Storfjorden from 22 to 24 March 2007. This was part of a full field program covering meteorology, sea ice, and oceanography with the icebreaker and coast-guard vessel K/V Svalbard from 18 to 31 March 2008 in northwestern Barents Sea. Under-ice boundary layer properties (velocity, conductivity, and temperature) in a strong tidal current environment were measured by two turbulence instrument clusters (TICs) and an Aanderaa Recording Doppler Current Profiler (RDCP) with concurrent hydrographical sampling by a SeaBird Electronics SBE19 CTD (conductivity, temperature, and depth) sonde from the ice camp on fast ice and in the polynya from K/V Svalbard. Figure 1 shows the bathymetry of Storfjorden with surrounding islands and the position of the ice camp (TICs and RDCP) and the CTD stations occupied during the campaign.

[9] The level ice in FMS was about 0.5 m thick, whereas the partly ridged ice exceeded 4 m in thickness. The two TICs were deployed 1 and 3 m below the level ice to measure turbulence properties in the under-ice boundary layer. Detailed description of the hydrographical survey and the under-ice sampling with the RDCP are given below, whereas the field measurement setup for the TICs is described in detail in a companion paper [*McPhee et al.*, 2013].

3.1. CTD

[10] A total of 37 CTD full-depth profiles were collected in Storfjorden using a SeaBird Electronics SBE19 (unpumped) sonde. The CTD-derived salinity is corrected against 20 salinity samples that were drawn with a 1.7 L Niskin bottle and analyzed with a Guildline Portasal 8410 salinometer resulting in an estimated uncertainty of 0.01 psu. The CTD accuracies provided by the manufacturer are 0.14 dbar, 0.005°C, and 0.0005 S m^{-1} for pressure, temperature, and conductivity, respectively. In order to avoid freezing of the sensors between stations, the CTD was kept in a heated box together with the Niskin bottle and the water sample bottles. The CTD sonde was first lowered to and maintained at 5–10 m depth until the measurements stabilized, then it was raised to just below the surface ready for profiling. Both downcast and upcasts were recorded. The sensor suite was lowered and raised at a speed in the range of 0.3–1.0 m s^{-1}, and the temperature and conductivity sensors were aligned in advance to pressure according to the descent rate of each cast.

[11] The hydrographic sampling program (Figure 1b) comprised four parts: (i) a closely spaced section (stations 2–12) about 15 km long, emanating from the fast ice camp in the afternoon of 23 March, coinciding with measurements at the ice camp during flood tide (i.e., flow into FMS); (ii) continuation of the section on the return to the fast ice camp in FMS on 24 March when conditions for CTD casting were better, starting in the deep basin (station 13), terminating with station 27 near the location of station 12, taken about 21 h earlier; (iii) a single station (station 28) at the deepest point (195 m) in the basin on 25 March after abandoning the fast ice camp on 24 March; and (iv) a section made on the way out of Storfjorden on 26 March (stations 29–37) across the western part of the sill at the entrance to the fjord.

3.2. RDCP

[12] The Aanderaa RDCP (RDCP 600) was deployed at 21:00 UTC on 22 March during ebb tide, strong wind, and snowdrift. The air temperature was −1°C, and the RDCP was suspended directly below 50 cm of level sea ice, facing downward. The conductivity and temperature sensors on the RDCP, with respectively accuracies of ±0.005 S m^{-1} and ±0.03°C, measured ∼2.5 m below the ice (∼3 m depth), whereas the current was measured every 2 m from ∼3.5 m below the ice (1 m blanking distance) down to the bottom (∼4 to 42 m depth). The freeboard was negative, i.e., the snow was covered with about 1 cm of sea water after the hole was drilled. Ice crystals emerged through the hole, and more than 1 m^3 of ice crystals (seawater drained out) had to be removed before the deployment was made. The instrument was recovered after 48 h, and current measurements show good quality for signal strength and standard deviations between the four beams down to the ocean floor at ∼45 m depth. Data sampling was set to burst mode using 400 pings every 5 min and a vertical bin size of 2 m. During the last 12 h, qualities of the temperature and conductivity (salinity) data gradually deteriorated due to low battery power and have been skipped.

4. Results

4.1. Hydrography

[13] The potential temperature versus salinity (θ−S) relationship for all hydrographical data collected in Storfjorden during the field campaign is shown in Figure 4. The data reveal a water column close to the freezing point relative to surface pressure in the polynya area and interior of Storfjorden. The TIC and RDCP points below the freezing point line (relative to surface pressure) are not realistic but indicate supercooling events and are pursued in more detail in a companion paper [*McPhee et al.*, 2013]. During the first part of the field campaign, the whole water column is BSW. The stability is clearly governed by the salinity, which is between 34.43 and 35.49 psu for the whole field campaign. The hydrographical profiles show that the water column close to the fast ice in FMS is colder and more saline than the water column at similar depths toward the interior of Storfjorden. The coldest and saltiest water is present between 70 and 90 m depths along the bottom toward the deeper basins in Storfjorden. Warmer water is present at intermediate depths above or next to the BSW overflow at the Storfjorden sill and mixes with surface and intermediate water inside Storfjorden all the way to FMS.

[14] Time series of temperature and salinity from the RDCP (∼2.5 m below the ice) and TIC1 (∼1 m below the ice) are given in Figure 5 and show that cold and saline BSW from the polynya area that has advected under the fast ice in FMS was gradually replaced by warmer and less saline water ($S < 34.8$ psu). Figure 6 shows the potential temperature and salinity profiles at stations 12 and 27 that are taken nearly at the same location but ∼21 h apart. The water column has become on average 0.08°C warmer and 0.27 psu less saline during these hours.

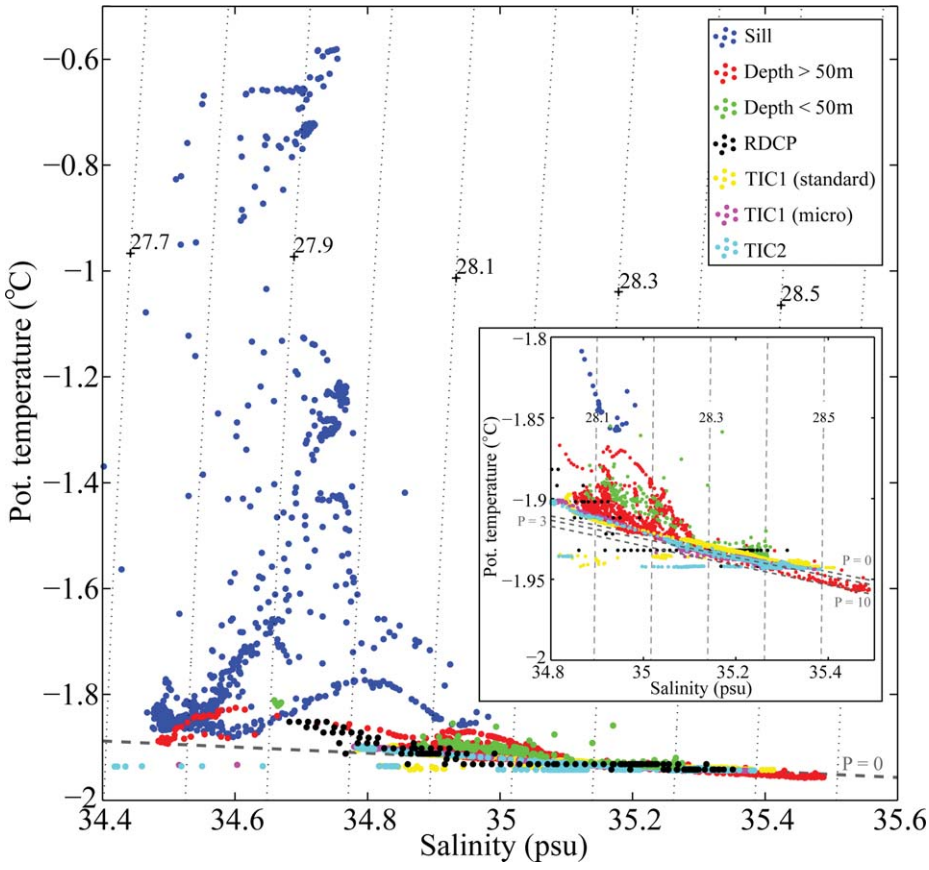

Figure 4. Potential temperature versus salinity diagram of all hydrographical data in Storfjorden during the K/V Svalbard cruise from 22 to 26 March 2007. Density ($\sigma_\theta = \rho_\theta - 1000$ kg m^{-3}) lines are drawn every 0.1 kg m^{-3}, and the freezing point temperature referred to the surface pressure is indicated by the dashed gray line. Expanded is a smaller low-temperature and high-salinity part with the freezing point temperature relative to surface, 3 dbar and 10 dbar indicated. CTD profiles from the sill are marked blue, CTD profiles from interior Storfjorden deeper than 50 m are marked red, and CTD profiles from the polynya area shallower than 50 m are marked green. Ice camp hydrographical time series from the RDCP, TIC1 standard conductivity, TIC1 microconductivity, and TIC2 are marked black, yellow, magenta, and cyan, respectively.

[15] Sections of S, θ, and σ_θ from FMS toward the interior of Storfjorden along the polynya length (stations 2–28) are presented in Figure 7. The colder and more saline water is seen at the shallow polynya area close to FMS behind the ~28 m deep ridge (Figure 1b) and is separated from the interior polynya water by warmer and less saline water in the upper 35–40 m between stations 26 and 5 on the other side of the ridge. The coldest and saltiest BSW is present between stations 18 and 24 along the bottom as a downflow toward the larger basins inside Storfjorden. Less saline BSW at deeper depths is present from other polynya events earlier in the freezing period. Details of the near-surface salinity front near the shallow ridge fronting FMS (stations 2–12) are discussed in section 3.2.

[16] Figure 8 shows the S, θ, and σ_θ sections across the western part of the main sill of Storfjorden (stations 29–37). Here warmer and less saline water with temperatures up to −0.5°C is present west of the cold and saline BSW overflow. The profiles are quite spiky in salinity which is mainly caused by the large gradients in temperature and hence giving problems with the processing of conductivity data. The salinity of the overflow is between 34.9 and 34.95 psu, and the profile just north of the sill (station 1, not shown) shows salinity of 34.95 psu, whereas the water in the deepest part of Storfjorden shows salinities between 35 and 35.1 psu.

4.2. Currents

[17] Currents in FMS were dominated by a strong semidiurnal tidal signal as illustrated by the 10 m depth measurement bin of the Aanderaa RDCP (Figure 9). The velocity vector is decomposed into an along sound velocity (Figure 9a, positive values into FMS) and an across sound velocity (Figure 9b) and shows that the dominating tidal signal is aligned along the sound axis with velocities exceeding 80 cm s^{-1}.

4.2.1. Tidal Analysis

[18] The RDCP data were split into barotropic and baroclinic time series by calculating the profile average for each time step and subtracting this average from the original time series. The M_2 component is the dominant tidal constituent and contains 95.1% of the total variance in the

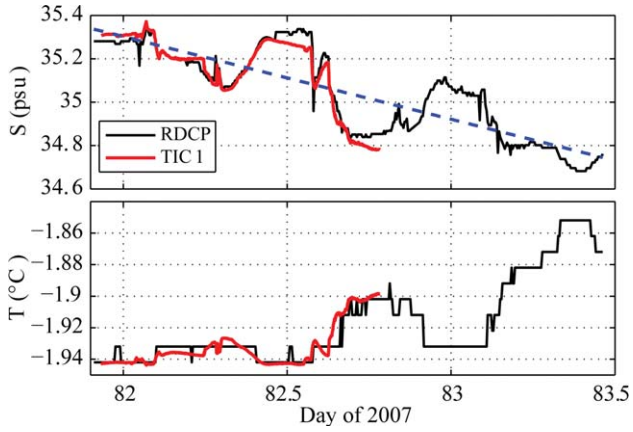

Figure 5. Salinity and temperature time series during the FMS deployment from 21:00 UTC on 22 March 2007, comparing the salinity and temperature time series for the RDCP profiler with the data from the first part of the deployment period by TIC1 [*McPhee et al.*, 2013] located 2.5 and 1 m below the ice-water interface, respectively. The blue dashed line shows the linear trend in salinity.

barotropic component and between 1% and 95% in the baroclinic component (Figure 10). The baroclinic signal is largest (relative to the total velocity variance) in the upper and lower parts of the velocity profile where it adjusts the barotropic signal toward the under-ice and bottom boundary layers. A change in the ellipse rotation and an amplitude increase are also visible around 24 m depth (Figure 10b), which reflect the depth of the submarine ridge in front of FMS (between stations 4 and 12 in Figure 7). The barotropic M_2 ellipse is orientated 41° counterclockwise relative to east. We then identified the major axis with the direction of the flood tide (into the sound from Storfjorden) as positive (i.e., bearing ~49°), the direction of the ebb tide

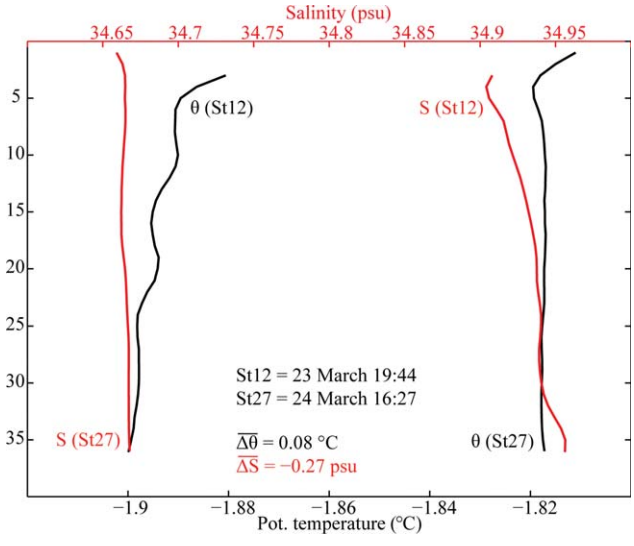

Figure 6. Salinity (red) and potential temperature (black) profiles at stations 12 and 27 obtained, respectively, on 23 and 24 March 2007 by the SBE19 sonde about 21 h apart at nearly the same location (see Figure 1).

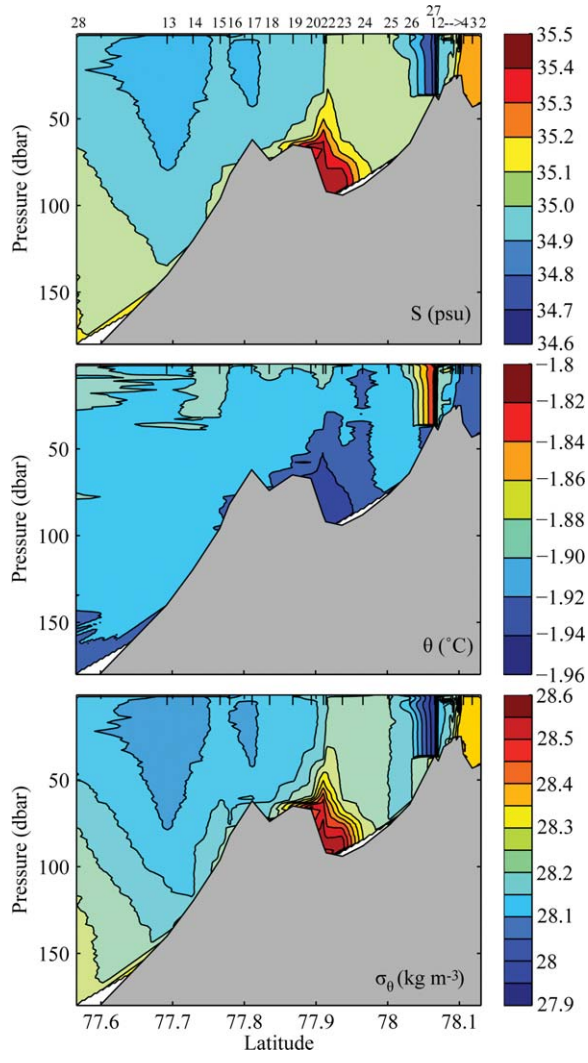

Figure 7. Sections of salinity (S), potential temperature (θ), and density ($\sigma_\theta = \rho_\theta - 1000$ kg m^{-3}) obtained on 23–25 March 2007 with the SBE19 sonde from station 2 at the fast ice edge in FMS to station 28 close to the deepest basin in Storfjorden (see Figure 1). Contours are given by the respective colorbars to the right.

(out of the sound) as negative (i.e., bearing ~229°), and the minor axis with the cross-channel flow (positive toward ~319° and negative toward ~139°).

4.2.2. Velocity Structure

[19] Along- and cross-channel flow components are plotted as contours in Figures 11 and 12, respectively. Removal of the barotropic (depth-averaged) flow reveals significant vertical structure in the baroclinic currents (Figures 11a and 12a) and a clear cross-axis circulation near the mouth of FMS with flow toward the northwest (positive) near the surface and southeast near the bottom (Figure 12a). This baroclinic circulation structure is strong during flood and weak during ebb. Periods with less vertical shear and nearly homogeneous velocity profile are visible during ebb episodes. Noticeably, a reduction in salinity and an increase in temperature are associated with the flood circulation pattern, whereas the opposite is associated with the ebb tide (Figures 11c and 12c).

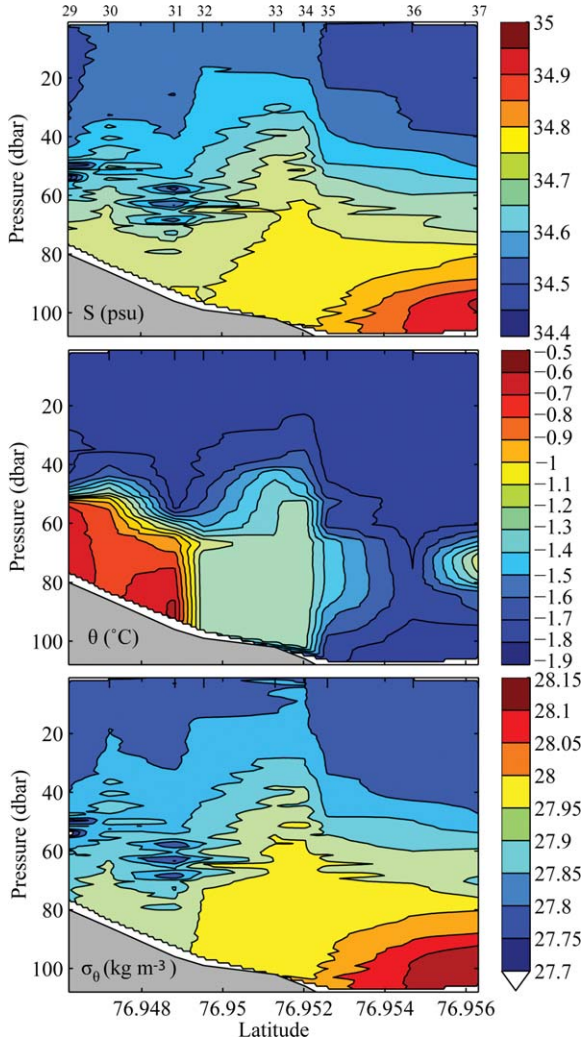

Figure 8. Sections of salinity (S), potential temperature (θ), and density ($\sigma_\theta = \rho_\theta - 1000$ kg m^{-3}) obtained on 26 March 2007 with the SBE19 sonde from stations 29 to 37 across the western part of the Storfjorden sill (see Figure 1). Contours are given by the respective colorbars to the right.

[20] In Figures 11b and 12b, the baroclinic tidal signal has been removed in each depth level, and the residual velocity is shown in the contourplots. Due to topographic enhancement of the tidal current in the shallow and narrow sound (FMS) combined with the boundary layer effects (both toward the bottom and the ice-water interface), we still see some tidal signal after removing the tidal components (from tidal harmonic analysis). Also, the southerly wind pulses increase/change the current through FMS during the measuring period. A relatively persistent negative cross-axis circulation is revealed in the layers below the ridge depth (below 24 m), and the surface velocities are reduced to near zero. The residual along-axis flow (Figure 11b) indicates a net flow into the sound (northeast) where the largest velocities are found around 10 to 20 m depth (above the ridge). The inflow is strongest and reaches 50 cm s^{-1} at the end of the time series and is associated with a general temperature increase and salinity decrease in the sound (Figure 11c).

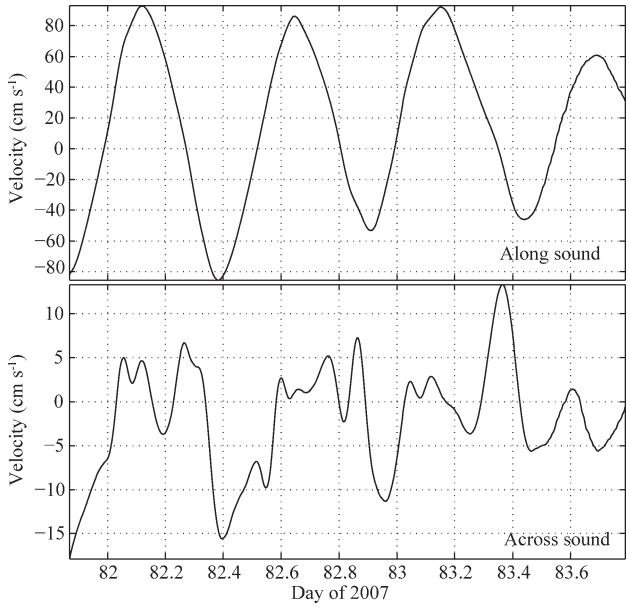

Figure 9. (upper) Along and (lower) across FMS velocity components from the 10 m depth bin for the RDCP obtained at the ice camp from 21:00 UTC on 22 March 2007.

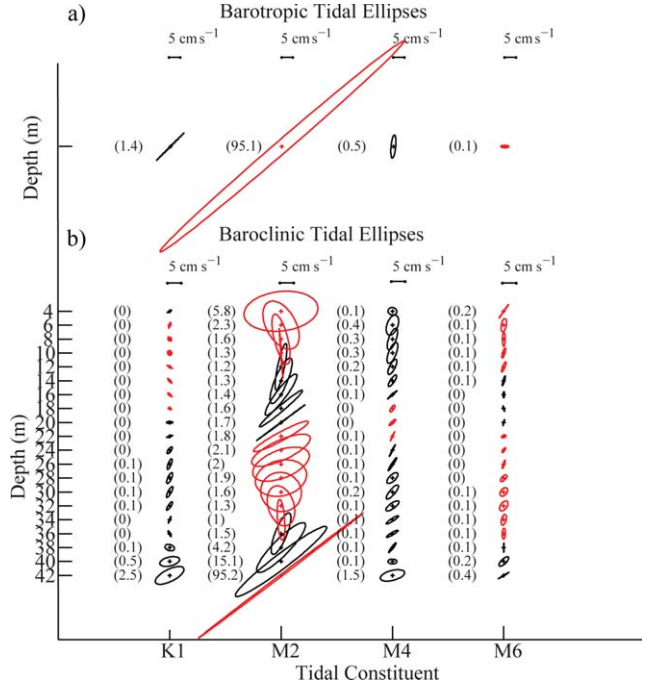

Figure 10. (a) Barotropic tidal ellipses of the four most dominating constituents in the RDCP velocity profile-averaged time series. Numbers indicate the percentage of the total barotropic variance. (b) Baroclinic tidal ellipses of the four most dominating constituents in the RDCP velocity profile time series after subtracting the depth-averaged profile time series. Numbers indicate the percentage of the total baroclinic variance. Black and red ellipses are cyclonic (+) and anticyclonic (−) rotation, respectively. The harmonic analysis was obtained by using T_TIDE in Matlab [*Pawlowicz et al.*, 2002].

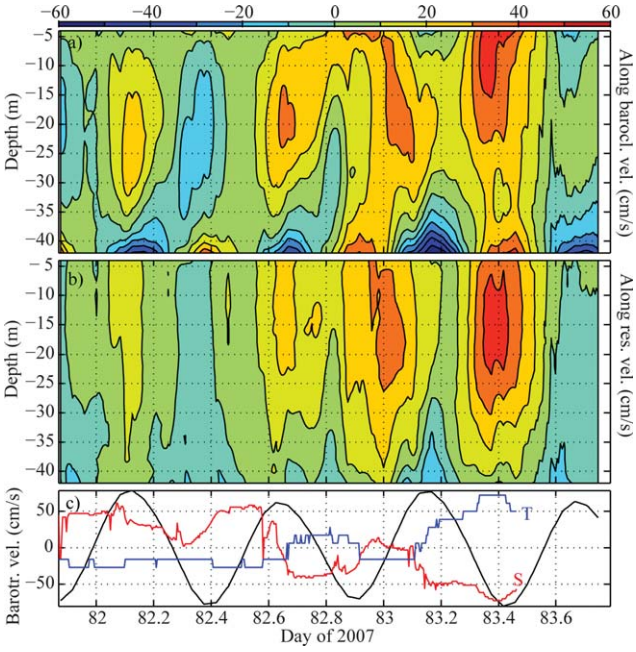

Figure 11. (a) Contourplot of baroclinic velocity (after subtracting the depth-averaged RDCP profile time series from the RDCP velocity profile time series) along FMS with depth and time. (b) Contourplot of residual velocity (after subtracting the barotropic and baroclinic tidal velocity) along FMS with depth and time. Contours are given by the colorbar on top. (c) Barotropic velocity along FMS (black), temperature (blue), and salinity (red) from the RDCP time series (see Figure 5 for temperature and salinity scales). All the time series are from 21:00 UTC on 22 March to 19:00 UTC on 24 March 2007.

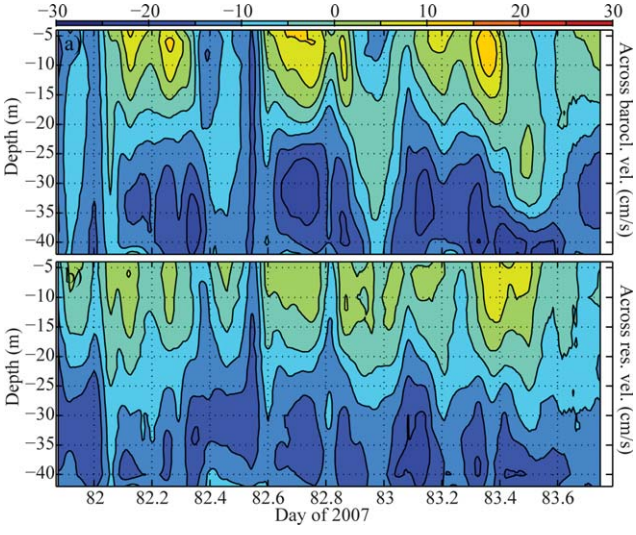

Figure 12. (a) Contourplot of baroclinic velocity (after subtracting the depth-averaged RDCP profile time series from the RDCP velocity profile time series) across FMS with depth and time. (b) Contourplot of residual velocity (after subtracting the barotropic and baroclinic tidal velocity) across FMS with depth and time. Contours are given by the colorbar on top. All the time series are from 21:00 UTC on 22 March to 19:00 UTC on 24 March 2007.

4.2.3. Horizontal Velocity Shear and Boundary Layer Thickness

[21] Figure 11 shows strong along-axis shear close to the upper and lower boundaries, and Figure 12 shows cross-axis shear within the water column. The shear has a strong tidal component, and maxima occur near the under-ice and bottom boundary layers, but there is also a strong shear near the central part of the water column around the ridge depth (~28 m), especially pronounced during flood periods (Figure 12a).

[22] Figure 13a shows the sum of the squared velocity shear representing the turbulence-producing denominator in the Richardson number. A minimum shear is clearly visible around ridge depth during entire ebb episodes, while the surface and bottom boundary layers show the same minimum at the end of each ebb episode. The echo amplitude measurements for the RDCP are shown in Figure 13b and will be used to indirectly indicate the stability of the water column.

5. Discussion

5.1. Polynya Activity Creating Cold and Saline Water

[23] The observed BSW (Figure 4) was likely produced by the polynya activity between 17 and 22 March 2007. This is supported by the satellite images in Figure 3. The Storfjorden polynya was opened by strong northerly winds during this period (days 76–81 in Figure 2). The accompanying large estimated net heat flux, exceeding 400 W m^{-2}, produced frazil ice that released brine to the underlying water in the polynya area. The maximum BSW salinity has been observed to vary interannually by more than unity,

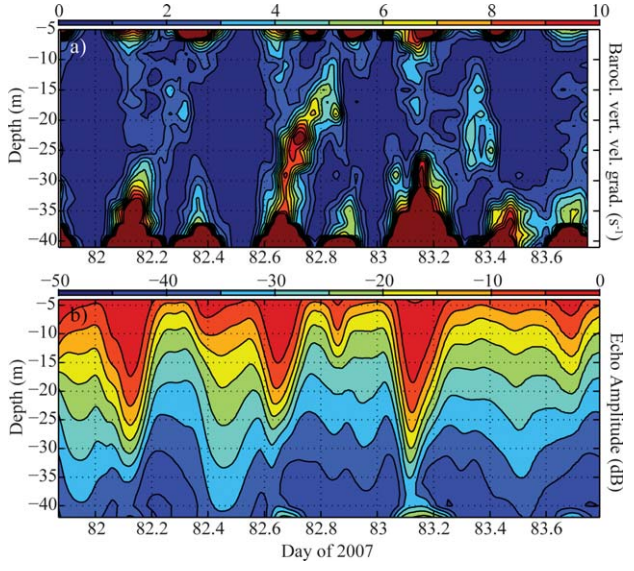

Figure 13. (a) Contourplot of the baroclinic vertical velocity gradient squared (velocity shear from Figures 11a and 12a after a 1 h boxcar running mean) in FMS with depth and time. (b) The RDCP echo amplitude measurements in FMS with depth and time. Contours are given by the colorbar on top of the respective panels. All the time series are from 22 March 21:00 UTC to 24 March 19:00 UTC.

and the density of BSW varies accordingly [*Skogseth et al*., 2005b]. Variations in atmospheric forcing over the polynya bring significant differences between winters and their sea ice cover, which has a huge impact on the source water of BSW [*Skogseth et al*., 2004]. The source water in Storfjorden is also influenced by varying inflow of saline water of Atlantic origin [*Schauer*, 1995; *Maus*, 2003; *Skogseth et al*., 2005b] due to the proximity to the Polar Front separating Arctic and Atlantic waters in the Barents Sea. The salinity of the observed BSW in March 2007 was average compared to other years but might have been higher at the end of the freezing period, since the source water salinity increases during the freezing period and large polynya activity in Storfjorden is normal in April as well [*Skogseth et al*., 2005a].

[24] The wind turned southerly with increasing force during the field campaign (days 81–85 in Figure 2). This influenced the presence of water masses in Storfjorden. In the surface, newly formed BSW was pushed toward the west coast of Edgeøya and under the fast ice in FMS and most likely through FMS and Heleysundet, whereas warmer and less saline water entering from the south was gradually replacing it. Figures 4 and 5 show that warmer water entered Storfjorden. This inflowing water from the south mixed with surface water inside Storfjorden all the way northward to FMS as seen by the temperature and salinity time series from the RDCP and TIC1 in Figure 5. Here cold and saline BSW from the most recent polynya area gradually got replaced by warmer and less saline water ($S < 34.8$ psu) entering Storfjorden from the south.

5.2. Sinking of Saline Water

[25] The coldest and saltiest water present at the slope between 70 and 90 m depths in front (southwest) of FMS (between stations 18 and 24 in Figure 7) is dense BSW likely produced during the most recent polynya activity flowing down toward the deeper parts of Storfjorden. The deepest profiles in Storfjorden show less saline BSW and indicate that the polynya activity prior to the last one produced less frazil ice or that the source water in the polynya was fresher while having likely greater entrainment of less saline water.

[26] Flow of BSW has been observed down the steepest topography from the shallow nearshore areas toward the deeper parts of Storfjorden just after an active polynya event [*Skogseth et al*., 2008]. This process fills up the deeper basins in Storfjorden with BSW, which eventually overflows the sill when the sill level is reached. Observations indicate a time lag of 12–18 days between the BSW production on the shallow polynya areas and the overflow at the sill [*Skogseth et al*., 2008]. Plumes of dense water originating from the Storfjorden polynya have been frequently observed south of the sill toward the shelf break of the West Spitsbergen Shelf [*Quadfasel et al*., 1988; *Anderson et al*., 1988; *Schauer*, 1995; *Schauer and Fahrbach*, 1999; *Fer et al*., 2003, 2004; *Fer*, 2006]. If its density permits, the plume cascades into the deep Norwegian Sea and northward along the eastern slope of Fram Strait toward the Arctic Ocean [*Quadfasel et al*., 1988].

5.3. Inflow and Circulation in Storfjorden

[27] The CTD section at the sill (Figure 8) shows the western part of the cold and saline BSW overflow. Warmer and less saline water is present west of the BSW overflow and is confined to the western slope of the sill, where the isopycnals indicate that this is a geostrophic adjusted current out of Storfjorden. Most likely, this is the return current of a geostrophic adjusted current into Storfjorden on the eastern part of the sill set up by the strong southerly winds during the field campaign. The *TS* diagram in Figure 4 shows that the BSW overflow mixes both isopycnally and diapycnally with the warmer and less saline water while approaching the sill. This is also visible from the CTD profiles showing that the BSW salinity decreases gradually from 35.1 psu at the deepest position (station 28), then to 34.95 psu just north of the sill (station 1, not shown) to 34.9–34.95 psu at the sill (Figure 8).

[28] The salinity increases and the temperature decreases in the surface layer (<50 m depth) from the sill area toward the shallow polynya area in front of FMS (Figure 4). The warmer and less saline surface water toward the sill area is due to inflow of warmer water from the south set up by an eastward Ekman transport and an accompanying surface elevation toward the west coast of Edgeøya and Barentsøya during the strong southerly wind event (Figure 2). The warmer and less saline inflow is seen between stations 4 and 25 in Figure 7 following the upper eastern slope of Storfjorden in front of FMS. Here a *TS* front (section 5.5) is created against colder and more saline BSW pushed toward the shallow coastal area along Edgeøya and into FMS. During the measuring period, this northward current became warmer and less saline as seen from Figures 5 and 6. The water column at station 27 is on average 0.08°C warmer and 0.27 psu less saline than at station 12 (Figure 6), which is taken ~21 h earlier at nearly the same location (Figure 1b).

[29] The above supports earlier indications of a general cyclonic circulation of water masses along the coast and topography inside Storfjorden [*Sjøkartverket*, 1990; *Schauer*, 1995; *Skogseth et al*., 2005b, 2007]. Numerical model studies have shown that the circulation in Storfjorden is very sensitive to wind forcing [*Skogseth et al*., 2007]. Ekman transports are easily set up during strong prevailing wind events affecting the mean transport direction through the ~0.6 km wide Heleysundet and the ~5.5 km wide FMS (Figure 1), even though strong tidal currents are present there. During northerly winds, a resulting westward Ekman transport sets up a southward geostrophic adjusted current following the coast and topography on the western side of the fjord and vice versa during periods with southerly winds. This leads to respectively sea level fall and rise inside Storfjorden near the sounds affecting the transport through them with a mean westward transport during sea level fall and a mean eastward transport during sea level rise. The mean transport through FMS during 4 days of observations in April 2004 with northerly wind was 0.05 Sv westward feeding the northern Storfjorden polynya area with source water from the northwestern Barents Sea [*Skogseth et al*., 2008]. As seen from Figure 11b, the southerly winds during the March 2007 field campaign caused an eastward transport through FMS. Using a mean residual current of 0.28 m s^{-1} during the measuring period, this gives a mean eastward transport of 0.08 Sv in line with earlier investigations.

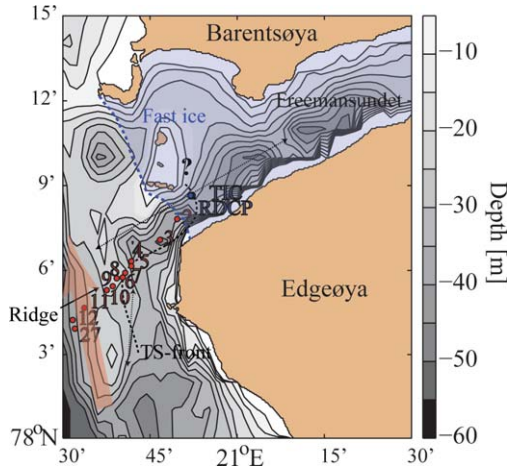

Figure 14. Detail of FMS bathymetry where the ice camp is indicated with blue dots (TIC and RDCP), and the locations of the densely spaced CTD stations in front of FMS are marked with red dots and corresponding station numbers. The fast ice area in FMS where the most recent polynya water is advected under is indicated with blue shaded color, where the dashed blue line indicates the fast ice border in front of FMS. The wind-induced northward current bringing warmer and less saline water from the south is illustrated by the red shaded arrow. The *TS* front separating this water from the colder and more saline polynya water is represented with the dashed black line. The dotted black double arrows indicate the tidal displacement along the major tidal axis into FMS. The location of the submarine ridge at about 28 m depth in front of FMS is also indicated. The boxed area in Figure 1b gives the border of the map. Bathymetry data are the same as in Figure 1b, and the contours are given in the colorbar.

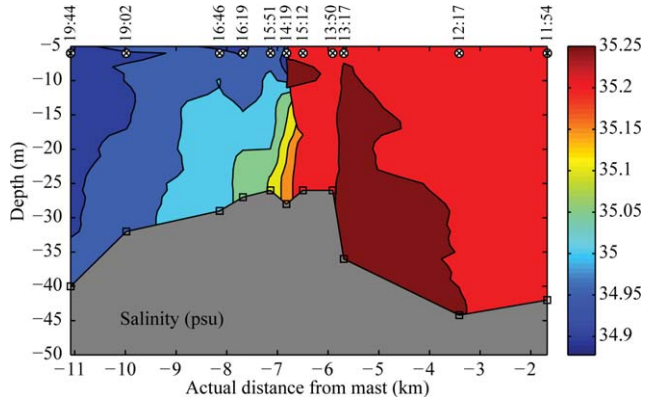

Figure 15. Detail of salinity structure near the mouth of FMS from a section of CTD stations (stations 2–12) directed away from the fast ice obtained on 23 March 2007 from 11:54 UTC to 19:44 UTC with the SBE19 sonde (see Figure 14). The occupation time of the stations is given on top, where the station positions are marked by white circles and black crosses. Distances are measured from the TIC deployment site along the major tidal axis oriented approximately NE. Contours are given by the colorbar to the right.

5.4. Advection of the Salinity Front

[30] Figure 14 shows details of bathymetry, ice camp features (RDCP and TICs), and station locations from the closely spaced section taken directly seaward (southwestward) of FMS on 23 March. Salinity structure during the survey (Figure 15) suggests that a sharp front is overlying the shallow (∼28 m depth) ridge at the entrance to FMS. As the CTD section progressed in time from about noon to late afternoon, currents increased at FMS from near slack to maximum flood at around 15:12 UTC and back to slack at about 18:30 UTC. The exact position of the frontal structure with time in the fairly topographically complex FMS area is not entirely clear as illustrated in Figure 14. But a progressive vector diagram (i.e., an estimate of water parcel displacement based on current measurements at the fixed ice camp location) provides context for interpreting the impact of advection on measurements made across the front as it moved with the tide (Figure 16). Near the mouth of FMS, displacement of about 12 km into the sound occurred during the time of the 23 March CTD survey, as indicated by the arrow in Figure 16. Earlier tidal analysis of the Storfjorden polynya area covering FMS using numerical model data [*Skogseth et al.*, 2007; E. A. Ersdal et al., On the tidal forcing of an Arctic coastal polynya, in preparation, 2013, hereinafter referred to as Ersdal et al., manuscript in preparation, 2013] gives that further north and south of FMS, the tidal displacement is much smaller and directed more north-south following the topography. Therefore, the frontal displacement must be accordingly smaller here as illustrated by the dotted arrows in Figure 14.

[31] As shown in Figure 5, the salinity front advected back and forth past our ice camp instruments with each successive flood/ebb cycle, where we observed a rectified wave signal in salinity with peak-to-trough amplitude of ∼0.3 psu, superimposed on a downward trend. The temperature changed accordingly with increasing peak-to-trough amplitude of ∼0.01°C to ∼0.08°C from beginning to end of the measuring period, superimposed on an upward trend. Nearly the same amplitude of variability for the surface layer temperature and salinity (∼0.3°C and 0.25 psu, respectively) associated with tidal-driven advection of a

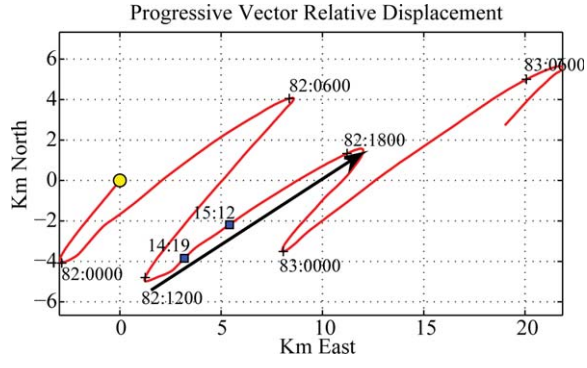

Figure 16. Progressive vector displacement of currents at middepth for the RDCP profile relative to the starting point at 21:00 UTC on March 2007 with day-of-year: hours indicated. The arrow indicates water column displacement during the 23 March CTD survey, and the time and relative position of station 6 (14:19 UTC) and station 7 (15:12 UTC) are indicated with blue squares.

directly polynya generated front through the land-fast-ice edge was reported by *Dmitrenko et al*. [2010]. The water column observed at the ice camp in FMS was initially very close to its salinity determined freezing temperature (relative to surface pressure) on both sides of the front, but by the end of ice camp measurements early on 24 March, temperature elevation above freezing had risen to ∼50 mK [*McPhee et al.*, 2013, Figure 1]. This coincided with the general trend of increasing temperature and decreasing salinity in the wind-induced inflow set up by the southerly wind event (section 5.3 and Figure 6).

[32] The contoured frontal structure shown in Figure 15 is complex, made more so by the fact that the measurements were separated in time as well as space. By assuming that the front moved in the direction of the survey line with water velocity somewhat like that measured by the RDCP in the upper 20 m at the ice camp, we applied a tidal displacement correction to the positions of the stations relative to the center of the front between station 6 obtained at 14:19 UTC and station 7 obtained at 15:12 UTC (Figure 17). This exercise, while only an approximation given the complex bathymetry of the ridge (Figure 14), suggests that the front is quite compact horizontally, and that the inshore water mass is well mixed, very close to its surface pressure freezing point. Since the survey started near slack tide at the end of an ebb cycle, this represents water advected out of FMS. On the Storfjorden side of the front, there is more stratification, with the entire water column between 10 and 30 mK above freezing. This is illustrated by individual stations on both sides of the front (Figure 18).

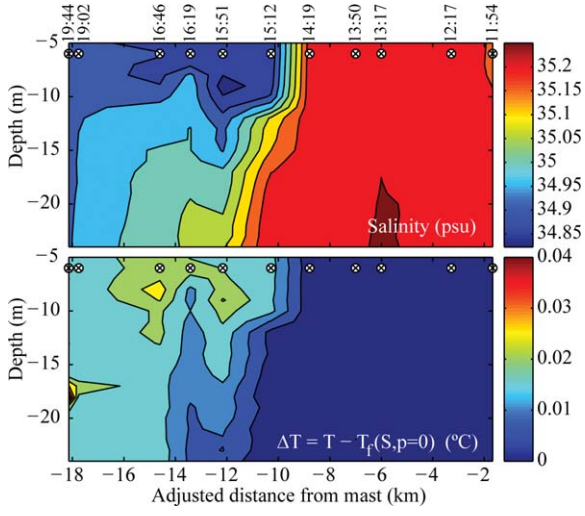

Figure 17. Sections of (upper) salinity and (lower) temperature elevation above freezing at surface pressure for the water column above ridge depth obtained on 23 March 2007 with the SBE19 sonde from station 2 (11:54 UTC) at the fast ice edge in FMS to station 12 (19:44 UTC) toward the deepest basin in Storfjorden (see Figure 1). The occupation time of the stations are given on top, where the station positions are marked by white circles and black crosses. Contours are given by the respective colorbars to the right. Distance is adjusted by time integrating the current obtained by the TIC mast at the ice camp using the occupation time of each CTD profile.

[33] The tidal advection of this front through ice-covered FMS generates an under-ice boundary layer with warmer and less saline (lighter) water underlying colder and more saline (heavier) water during flood and vice versa during ebb. Hence, the under-ice water column gets unstable during flood and stable during ebb. This effect is indicated in Figure 13, where the echo amplitude from the RDCP is elevated down to around ridge depth (∼25 to 30 m depth) during flood and strongly reduced during ebb. The RDCP is receiving reflected acoustic signals from suspended particles in the water column, and large echo amplitudes indicate high number of suspended particles as sediments, biological matter, or frazil ice crystals. During the deployment of the RDCP, large amount of frazil ice crystals was present in the water under the ice (section 3.2), suggesting that the elevated echo amplitude in Figure 13 might be due to frazil ice crystals. If so, they were transported down the water column due to enhanced turbulence during flood (unstable water column) and confined close to the ice-water interface due to suppressed turbulence during ebb (stable water column). This process could generate an "ice-pump" mechanism as long as the water column is at the freezing point temperature relative to surface pressure. So, during flood, frazil ice would then be mixed down and melted in a water column initially at surface freezing, and the heat extracted would drive the temperature toward in situ freezing. It is notable that the water column east of the front (station 2) is uniformly near its surface freezing temperature, indicating an absence of ice melting at depth at the fast ice edge by the ice camp in FMS. Unfortunately, no time series of full-depth temperature and salinity profiles were obtained in close vicinity of the RDCP site that can support or reject this.

5.5. Tidal Flow and Mixing in FMS

[34] Tidal currents are generally strong in the sounds in the northern part of Storfjorden. Speeds of 4–5 and 2–3 m s^{-1} are reported in Heleysundet and FMS, respectively [*Sjøkartverket*, 1990]. These currents exert a large stress on the ice cover and help break off the land-fast ice outside the sounds [*Zyryanov et al*., 2003]. The strong currents further redistribute the ice and keep the polynya open even during calm wind periods contributing to increased ice production (Ersdal et al., manuscript in preparation, 2013). The strong tidal currents through the sounds are set up by a half-phase shift between Storfjorden and the northwestern Barents Sea [*Gjevik et al*., 1994; *Skogseth et al*., 2007]. When the tidal bulge propagates southward in the Barents Sea and enters the sounds, a relatively low sea level in Storfjorden enhances the strength of the tidal current through them. The M_2-dominated tidal current propagating through ice-covered FMS was observed to peak at 53 cm s^{-1} during 4 days of observations in April 2004, producing shallow water components and a locally well-mixed water column [*Skogseth et al*., 2008]. FMS experienced even stronger tidal currents during the March 2007 field campaign, where the major M_2 axis reached 72 cm s^{-1} (Figure 10), and the total barotropic oscillation peaked at 80 cm s^{-1}. As shown in Figure 13a, these strong currents create strong velocity shear in the under-ice and bottom boundary layers. This shear represents the turbulence-producing denominator in the Richardson number. The numerator in the Richardson number is

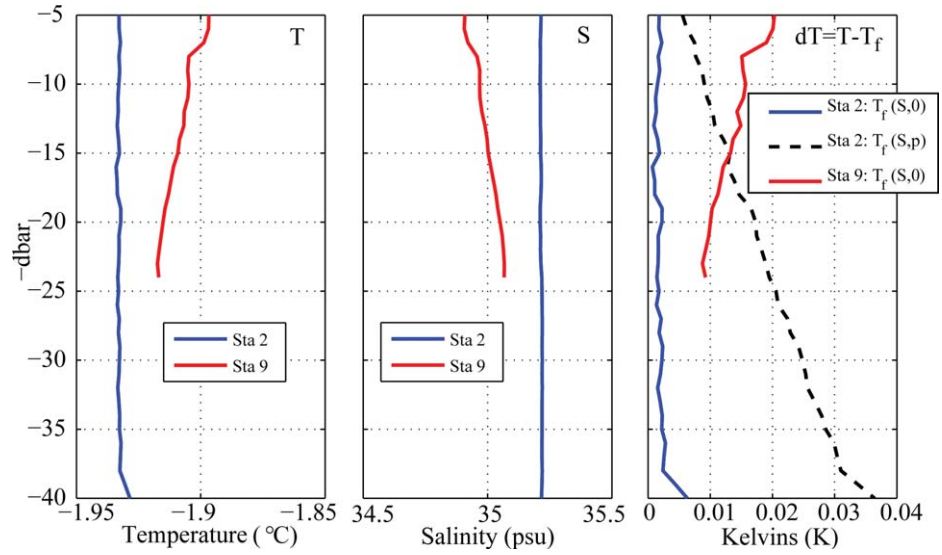

Figure 18. Comparison of temperature (T), salinity (S), and elevation of temperature above freezing (kelvin) profiles (from average of downcasts and upcasts) taken near the fast ice edge at 11:54 UTC on (station 2) and seaward of the front at 16:19 UTC (station 9) on 23 March 2007. For station 2, the elevation of temperature above freezing is shown relative to surface pressure ($T_f(S, 0)$, solid blue) and at in situ pressure ($T_f(S, p)$, dashed black).

given by the vertical density gradient or the strength of the stratification in the water column. Due to the dependency of suspended particles in the water column, the echo amplitude measurements for the RDCP shown in Figure 13b can be used to indicate changes in the stability of the water column and the boundary layer development with time. The echo amplitude time series show an increased mixed layer depth and possible transient destabilization of the water column during flood and a shallow mixed layer depth and likely stable stratification during ebb episodes. At low temperatures, the stratification is mainly governed by the salinity. From the RDCP salinity (temperature) time series in Figure 13c, we see that the salinity (temperature) ~2.5 m below the ice is mainly decreasing (increasing) during flood and increasing (decreasing) during ebb. Unfortunately, no full-depth time series of temperature and salinity were obtained to confirm this, but since the water column is well mixed on both sides of the front (Figures 17 and 18) this likely signifies a *TS*-front passage in and out of FMS creating, respectively, unstable and stable stratification in the under-ice boundary layer.

[35] The flow response in FMS can be understood by assessing the residual or nontidal current (Figure 11b and 12b) which shows a dominating southeastern current from the bottom up to approximately 15 m depth throughout the time series. When comparing the residual current direction with the topography below the RDCP in FMS (Figure 14), the residual current seems to be topographically steered cyclonically around a deeper depression.

5.6. Implications of Double Diffusion

[36] The θS diagram (Figure 4) shows some events measured by the TICs and the RDCP where the temperature is below surface freezing point temperature. The amount of supercooling is unrealistic, but the events are indications of transient supercooling. *McPhee et al.* [2013] present evidence that differential mixing of salt and heat (double diffusion) between two water masses of differing salinity, each very close to freezing, can lead to transient supercooling events, with the possibility of frazil production, provided adequate nucleation sites exist.

[37] Given that the double-diffusion process operates, this suggests a novel frazil ice production process in tidally induced coastal polynyas that depends on frontal dynamics rather than direct contact with the atmosphere. Tidally induced coastal polynyas are present all over the Arctic continental shelf area [*Windsor and Björk*, 2000; *Hannah et al*., 2009] where saline, near-freezing water is produced in the open polynya water creating salinity fronts against surrounding water under the fast or pack ice [*Shcherbina et al*., 2004; *Dmitrenko et al*., 2010]. The tides will advect these fronts under the ice cover and create under-ice boundary layers favoring double diffusion across the interface between saline, cold polynya water and less saline, warmer water, both near their respective freezing point temperature. During the double-diffusion process, the warmer and less saline water will lose heat faster than it gains salt, so the water gets supercooled and frazil ice can grow. The large-scale effect of this is most likely small when considering the difference in net heat flux in a typical polynya event with surface cooling and in double diffusion with very small temperature gradients. During the polynya event prior to the field campaign in FMS, the estimated net heat flux from ocean to atmosphere reached 400 W m^{-2}, while the heat flux in the double diffusion was about 3 W m^{-2} [*McPhee et al.*, 2013]. A supercooling event with temperature reaching 0.037°C below freezing point temperature relative to surface pressure has been measured during surface cooling in the Storfjorden polynya [*Skogseth et al*., 2009]. Water temperature 0.02°C below freezing relative to surface has been measured in the Laptev Sea polynya [*Dmitrenko et al*., 2010]. The small heat flux in the double-

diffusion process will give a much smaller degree of supercooling ($O(10^{-3})$) and therefore, much smaller frazil ice crystals than during surface cooling. Even though the frazil ice production due to double diffusion in the under-ice boundary layer is small and perhaps negligible compared to the frazil ice production due to surface cooling in a polynya, the frazil ice production due to double diffusion will happen as long as a salinity front is present with water near freezing during both opening and closing of polynyas, and might be an important integrated contribution to the total ice production in a polynya area.

6. Conclusion

[38] A new set of observations from the Storfjorden Polynya on the eastern side of the Svalbard Archipelago from March 2007 has been presented here. The observations confirm that the polynya produces sea ice during periods of intense heat loss (estimated to exceed 400 W m^{-2}), and releases brine so that the resulting water at the freezing point reaches a salinity of ~35.5 psu and a density of ~1028.6 kg m^{-3}. This dense brine-enriched water at the freezing point mixes with warmer and less saline water entering from the south on its way out of the fjord and leaves as a dense bottom layer at the sill with properties ~34.9 psu, −1.8°C and ~1028.1 kg m^{-3}.

[39] Following such an intense polynya event, the atmosphere warmed toward 0°C, and winds turned southerly pushing the cold saline polynya water and frazil ice northward and eastward under the fast ice in a nearby narrow sound. The southerly winds induced a northward current gradually bringing slightly warmer and less saline water into Storfjorden and the ice-covered narrow sound. This created an abrupt salinity front between the fresher and warmer water entering the area from the south and the brine-enriched colder water produced earlier by the polynya. We observed this abrupt salinity front as it advected into the narrow ice-covered sound where it experienced intense mixing due to flow exceeding 80 cm s^{-1} along the direction of the sound. This flow had a strong baroclinic shear related to local topography and the fixed boundary layers at the top (fast ice) and bottom of the water column. Enhanced turbulent mixing during flood events and suppressed turbulent mixing during ebb were indirectly observed due to the effects of frontal advection, under-ice boundary layer, and stratification. The small-scale turbulence is substantiated in the companion paper by *McPhee et al.* [2013].

[40] As the front passes the location of the instruments, some unexpected transient supercooling effects occur. Small-scale details and the correct level of supercooling are also described by *McPhee et al.* [2013]. Regardless of these details, the water in the sound is intensely mixed, and frazil ice crystals are present in the upper part of the column. The observations therefore document that supercooling can persist away from the intense heat fluxes that created it and indicate that frazil ice crystals may exist for days after they have formed. This persistence of supercooling and frazil ice crystals is likely a general process that occurs in many Arctic and Antarctic polynyas given that some of the BSW is advected below thicker ice. A small and new volume of frazil ice may also grow from the suggested double-diffusion process [*McPhee et al.*, 2013]. Even though this ice growth and supercooling are several orders of magnitude smaller than that in the open polynya, it may indeed create challenges with respect to observations and also application of "standard" turbulence theory.

[41] **Acknowledgments.** This work has been funded by the IPY project Bipolar Atlantic Thermohaline Circulation (BIAC) and the Storfjorden Polynya Air Sea Ice Exchange Experiment (POLRES grant 196145 from the Norwegian Research Council to R. Skogseth and F. Nilsen at the University Centre in Svalbard and L. H. Smedsrud at Uni Research, and NSF grant NSF ARC-0906820 to M. G. McPhee at McPhee Research Co). We thank two anonymous reviewers for constructive comments and suggestions improving this manuscript. We thank the captain and crew at the Norwegian coastguard vessel K/V Svalbard for superb service and invaluable help during the FMS field campaign.

References

Aagaard, K., L. K. Coachman, and E. Carmack (1981), On the halocline of the Arctic Ocean, *Deep-Sea Res. Part A*, *28*, 529–545.

Anderson, L. G., E. P. Jones, R. Lindegren, B. Rudels, and P.-I. Sehlstedt (1988), Nutrient regeneration in cold, high salinity bottom water of the Arctic shelves, *Cont. Shelf Res.*, *8*, 1345–1355.

Daly, S. F. (1984), Frazil Ice Dynamics, U.S. Army Cold Reg. Res. Eng. Lab., CRREL Monogr., 84–1, Hanover, N. H.

Dmitrenko, I. A., et al. (2010), Observations of supercooling and frazil ice formation in the Laptev Sea coastal polynya, *J. Geophys. Res.*, *115*, C05015, doi:10.1029/2009JC005798.

Dmitrenko, I. A., S. A. Kirillov, E. Bloshkina, and Y.-D. Lenn (2012), Tide-induced vertical mixing in the Laptev Sea coastal polynya, *J. Geophys. Res.*, *117*, C00G14, doi:10.1029/2011JC006966.

Fer, I. (2006), Scaling turbulent dissipation in an Arctic fjord, *Deep-Sea Res. Part II*, *53*, 77–95.

Fer, I., R. Skogseth, P. M. Haugan, and P. Jaccard (2003), Observations of the Storfjorden overflow, *Deep-Sea Res. Part I*, *50*(10–11), 1283–1303.

Fer, I., R. Skogseth, and P. M. Haugan (2004), Mixing of the Storfjorden overflow (Svalbard Archipelago) inferred from density overturns, *J. Geophys. Res.*, *109*(C1), C01005, doi:10.1029/2003JC001968.

Gawarkiewicz, G., and D. C. Chapman (1995), A numerical study of dense water formation and transport on a shallow, sloping continental shelf, *J. Geophys. Res.*, *100*, 4489–4508.

Gjevik, B., E. Nøst, and T. Straume, (1994), Model simulations of the tides in the Barents Sea, *J. Geophys. Res.*, *99*, 3337–3350.

Haarpaintner, J., J. C. Gascard, and P. M. Haugan (2001), Ice production and brine formation in Storfjorden, Svalbard, *J. Geophys. Res.*, *106*, 14,001–14,013.

Hannah, C. G., F. Dupont, and M. Dunphy (2009), Polynyas and tidal currents in the Canadian Arctic Archipelago, *Arctic*, *62*(1), 83–95.

Ingram, R., J. Bacle, D. Barber, Y. Gratton, and H. Melling (2002), An overview of physical processes in the North Water, *Deep-Sea Res. Part II*, *49*, 4893–4906.

Liu, A. K., S. Martin, and R. Kwok (1997), Tracking of ice edges and ice floes by wavelet analysis of SAR images, *J. Atmos. Oceanic Technol.*, *14*, 1187–1198.

Maus, S. (2003), Interannual variability of dense shelf water salinities in the north-western Barents Sea, *Polar Res.*, *22*, 59–66.

Maykut, G. (1986), The surface heat and mass balance, in: *The Geophysics of Sea Ice*, edited by N. Untersteiner, Plenum, New York.

McPhee, M. G., R. Skogseth, F. Nilsen, and L. H. Smedsrud (2013), Creation and tidal advection of a cold salinity front in Storfjorden. Part 2: Supercooling induced by turbulent mixing of cold water, *J. Geophys. Res. Oceans*, *118*, doi:10.1002/jgrc.20261.

Quadfasel, D., B. Rudels, and K. Kurz (1988), Outflow of dense water from a Svalbard fjord into the Fram Strait, *Deep-Sea Res.*, *35*, 1143–1150.

Pawlowicz, R., B. Beardsley, and S. Lentz (2002), Classical tidal harmonic analysis including error estimates in MATLAB using T_TIDE, *Comput. Geosci*, *28*, 929–937.

Schauer, U. (1995), The release of brine-enriched shelf water from Storfjord into the Norwegian Sea, *J. Geophys. Res.*, *100*, 16,015–16,028.

Schauer, U., and E. Fahrbach (1999), A dense bottom water plume in the western Barents Sea: Downstream modification and interannual variability, *Deep-Sea Res. Part I*, *46*, 2095–2108.

Shcherbina, A. Y., L. D. Talley, and D. L. Rudnick (2004), Dense water formation on the northwestern shelf of the Okhotsk Sea: 1. Direct

observations of brine rejection, *J. Geophys. Res.*, *109*, C09S08, doi:10.1029/2003JC002196.

Sjøkartverket (1990), *Arctic Pilot Sailing Directions Travellers' Guide Svalbard and Jan Mayen*, *2nd ed.*, vol. *7*, The Norw. Hydrogr. Serv. and Norw. Polar Res. Inst., Norway.

Skogseth, R., P. M. Haugan, and J. Haarpaintner (2004), Ice and brine production in Storfjorden from four winters of satellite and in situ observations and modeling, *J. Geophys. Res.*, *109*, C10008, doi:10.1029/2004JC002384.

Skogseth, R., I. Fer, and P. M. Haugan (2005a), Dense-water production and overflow from an Arctic coastal polynya in Storfjorden, in *The Nordic Seas: An Integrated Perspective*, edited by H. Drange, T. Dokken, T. Furevik, R. Gerdes and W. Berger, *Geophys. Monogr. Ser.*, vol. *158*, pp. 73–88, AGU, Washington, D. C., doi: 10.1029/158GM07.

Skogseth, R., P. M. Haugan, and M. Jakobsson (2005b), Watermass transformations in Storfjorden, *Cont. Shelf Res.*, *25*, 667–695.

Skogseth, R., A. L. Sandvik, and L. Asplin (2007), Wind and tidal forcing on the meso-scale circulation in Storfjorden, Svalbard, *Cont. Shelf Res.*, *27*, 208–227, doi:10.1016/j.csr.2006.10.001.

Skogseth, R., L. H. Smedsrud, F. Nilsen, and I. Fer (2008), Observations of hydrography and downflow of brine-enriched shelf water in the Storfjorden polynya, Svalbard, *J. Geophys. Res.*, *113*, C08049, doi:10.1029/2007JC004452.

Skogseth, R., F. Nilsen, and L. H. Smedsrud (2009), Supercooled water in an Arctic polynya: Observations and modeling, *J. Glaciol.*, *55*(189), 43–52.

Smith, S. D., R. J. Anderson, G. Den Hartog, D. R. Topham, and R. G. Perkin (1983), An investigation of a polynya in the Canadian Archipelago: 2. Structure of turbulence and sensible heat flux, *J. Geophys. Res.*, *88*(C5), 2900–2910.

Smith, S. D., R. D. Muench, and C. H. Pease (1990), Polynyas and leads: An overview of physical processes and environment, *J. Geophys. Res.*, *95*, 9461–9479.

Williams, W. J., E. C. Carmack, and R. G. Ingram (2007), Physical oceanography of polynyas, in *Polynyas: Windows to the World*, edited by W. O. Smith and D. G. Barber, Elsevier Oceanogr. Ser., vol. *74*, pp. 55–86, Elsevier, Amsterdam.

Windsor, P., and G. Björk (2000), Polynya activity in the Arctic Ocean from 1958 to 1997, *J. Geophys. Res.*, *105*(C4), 8789–8803.

Topham, D. R., R. G. Perkin, S. D. Smith, R. J. Anderson, and G. Den Hartog (1983), An investigation of a polynya in the Canadian Archipelago: 1. Introduction and oceanography, *J. Geophys. Res.*, *88*(C5), 2888–2899.

Zyryanov, D., J. Haarpaintner, and R. Korsnes (2003), Numerical modelling of the Storfjorden (Svalbard) polynya development due to wind stress: Role of the sea ice rheology and damping forces, *Polar Res.*, *22*(2), 235–245.